Numerical Study of the Effects of the Great Lakes on a Winter Cyclone

MAURICE B. DANARD and GANDIKOTA V. RAO [1]—*University of Waterloo, Waterloo, Ontario, Canada*

ABSTRACT—A vigorous winter storm over North America is studied by means of an eight-level primitive-equation model. Included are orography, surface and internal friction, long-wave radiation from clouds and water vapor, large-scale release of latent heat, and fluxes of sensible heat and water vapor from water surfaces. Sigma coordinates are employed. The grid size is 190 km at 60°N.

Two 36-hr numerical integrations are performed, one with and one without the effects of the Great Lakes and other water surfaces. When these influences are included, lower tropospheric temperatures are raised by more than 7°C and 1000-mb heights are reduced as much as 70 m.

Ekman layer wind speeds are modified by up to 6 m/s. The maximum increase in large-scale precipitation over the Great Lakes is 0.5 cm with decreases to the southeast. Below 800 mb, isobaric surfaces are lowered; they are raised at higher levels. Effects on vorticity and divergence also change sign between lower and upper troposphere. Near the earth's surface, the average contribution of the Great Lakes is 1.9×10^{-5} s^{-1} to the vorticity and -1.5×10^{-5} s^{-1} to the divergence. The associated effects on both the rotational and divergent wind fields amount to about 3 m/s.

1. INTRODUCTION

A number of studies have been made on the small-scale effects of the Great Lakes (e.g., snowbelts). A review of these has recently been written by the authors (Rao and Danard 1971). However, comparatively few investigations have dealt with influences on large-scale atmospheric circulations. Petterssen (1950) showed that the Great Lakes region has a high frequency of cyclones in winter but not in summer. This was attributed to heating of arctic air masses in the cold season by the unfrozen lakes. He later commented (Petterssen 1956, p. 326) that "when a cyclone disturbance approaches the Great Lakes in winter, additional development is often observed to take place in advance of the center. As the center moves out of the lake region, the development intensifies in the rear, with the result that the progress of the cyclone center is retarded. This accounts for the high frequency of cyclone centers over the Great Lakes (and other inland water bodies) during the cold season." Petterssen and Calabrese (1959) computed that a relative geostrophic vorticity maximum of about 4×10^{-5} s^{-1} was produced at the surface by the Great Lakes within 48 hr during cold air outbreaks. Further increases in cyclonic vorticity would tend to be offset by friction. The probable upper limit was estimated to be about 1×10^{-4} s^{-1}. The corresponding maximum drop in surface pressure due to heating over the Great Lakes would be 6 or 7 mb.

This paper is concerned with determining, by numerical simulation, the effects of the Great Lakes on large-scale atmospheric motions. The eight-level primitive-equation

model of Danard (1971) is modified as described in sections 2 and 3. First, the grid size is halved. Second, vertical fluxes of sensible heat and water vapor from water surfaces are included in the lower troposphere.

The revised model is applied to a vigorous winter cyclone. Results are discussed in section 4. Two 36-hr numerical prognoses are prepared, one with and one without the influences of the Great Lakes and other water bodies.

2. GENERAL DESCRIPTION OF THE MODEL

The model is an adaptation of the one described by Danard (1971). The latter model employs sigma coordinates and includes orography, surface and internal friction, long-wave radiation, and large-scale release of latent heat. The σ-levels at which the geopotential, ϕ, velocity components, u and v, vertical velocity, $\dot{\sigma} = d\sigma/dt$, temperature, T, and mixing ratio, r, are computed are shown in figure 1. Here, $\sigma = p/p_s$ where p is the pressure and p_s is the pressure at the earth's surface.

Two important changes have been made for the present study. First, the grid size has been halved (it is now 190 km at 60°N). This reduces truncation error, but the size of the forecast region has also been decreased. Second, sensible heat flux and evaporation from water surfaces have been included. This permits a study of the large-scale effects of the Great Lakes.

The water temperature for the Great Lakes gridpoints is set equal to 33°F. This may be compared to the mean February and March values given by Richards and Irbe (1969) of 34° and 33°F, respectively.
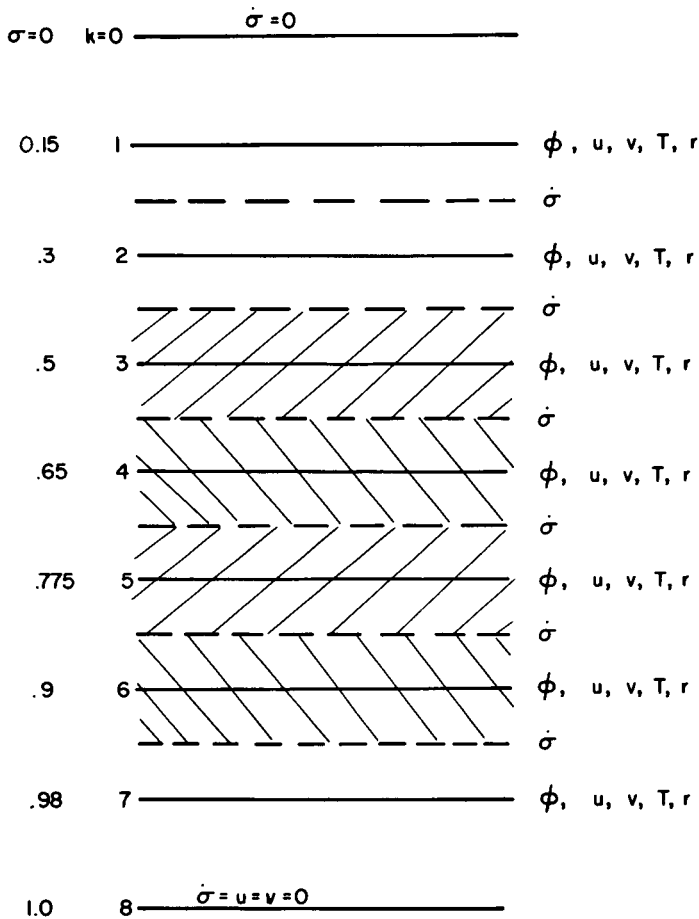
FIGURE 1.—Levels at which variables are computed. Cross-hatching indicates layers where cloud and precipitation may occur.
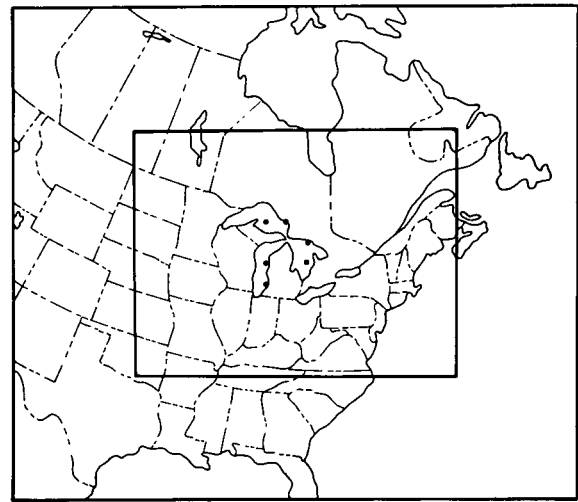

FIGURE 2.—Map showing area specified initially (outer border) and area of viable forecast (inner border). Gridpoints representing ice-free surfaces on the Great Lakes are shown as dots.

The forecast area and gridpoints representing the Great Lakes are shown in figure 2. The outer border delineates the area occupied by the 24×28 gridpoints for which initial data are given. Forecast maps (figs. 3–12) are prepared for the 12×16 points inside the inner border. As in the earlier study (Danard 1971), initial data consist of heights at 1000, 850, 700, 500, and 300 mb and temperatures and dew-point temperatures at 850, 700, and 500 mb.

To obtain terrain heights for this model, we used the elevations at 1° latitude-longitude intersections (Berkofsky and Bertoni 1960) to compute the mean heights for 2° latitude-longitude "squares." These were then analyzed and the height read off at gridpoints.

In this model, the Great Lakes have three influences. First, they constitute a warm radiating surface and thus supply heat. Second, they yield sensible heat to and destabilize the lower troposphere. Third, they provide water vapor. None of these was included for the Great Lakes in the earlier model (Danard 1971), although the first process was incorporated for ocean areas.

The equations used in the present model are identical to those of Danard (1971) except for his eq (3) and (4) (first law of thermodynamics and the moisture equation).

Those are replaced by

$$\frac{\partial}{\partial t} p_s T = -m^2 \left(\frac{\partial}{\partial x} \frac{p_s u T}{m} + \frac{\partial}{\partial y} \frac{p_s v T}{m} \right) - p_s \frac{\partial}{\partial \sigma} \dot{\sigma} T$$
$$+ \frac{RT\omega}{c_p \sigma} + \frac{p_s}{c_p} \left(H_L + H_R + H_s \right) + m^2 K_T \nabla^2 p_s T \quad (1)$$

and

$$\frac{\partial}{\partial t} p_s r = -m^2 \left(\frac{\partial}{\partial x} \frac{p_s u r}{m} + \frac{\partial}{\partial y} \frac{p_s v r}{m} \right) - p_s \frac{\partial}{\partial \sigma} \dot{\sigma} r$$
$$+ p_s (W - C) + m^2 K_r \nabla^2 p_s r. \quad (2)$$

The terms H_s and W are the only additional ones and represent, respectively, the rate of input of heat per unit mass from sensible heat flux and rate of increase of r due to evaporation from a water surface. The map factor is denoted by m, R is the gas constant, c_p is the specific heat at constant pressure, $\omega = dp/dt$, K_T and K_r are eddy diffusivities, H_L and H_R are the rates of input of heat per unit mass due to latent heat release and long-wave radiation, and C is the rate of decrease of r caused by condensation. The computation of H_s and W is described in section 3.

The method of initialization, boundary conditions, finite differences used, and the values assigned to the eddy diffusivities are the same as in Danard (1971). However, the time step has been halved to 5 min as necessitated by the reduced grid size.

3. COMPUTING THE EFFECTS OF SENSIBLE HEAT FLUX AND EVAPORATION FROM A WATER SURFACE

The turbulent fluxes of sensible heat, F_{so}, and water vapor, F_{wo}, through a unit horizontal area at a water surface are computed by slightly modifying the semi-empirical transfer equations (e.g., Roll 1965, p. 252). Here, we

use

$$F_{s0} = \rho C_D c_p V_7 (T_s - T_a) \qquad (3)$$

and

$$F_{w0} = \rho C_D V_7 (r_s - r_7) \qquad (4)$$

In the above, ρ is the air density, C_D is the drag coefficient (assigned the value of 1.3×10^{-3} as suggested by Cressman 1960 for a water surface), V_7 is the wind speed at level 7 (approx. 200 m above the surface, fig. 1), T_s is the temperature of the water surface, T_a is the surface air temperature (obtained by extrapolation from levels 6 and 7 assuming that T varies linearly with ln p), r_s is the saturation mixing ratio corresponding to T_s, and r_7 is the mixing ratio at level 7 (assumed equal to that at the surface). If $T_s \leq T_a$, then $F_{s0} = 0$. Similarly, if $r_s \leq r_7$, then $F_{w0} = 0$.

The fluxes are assumed to decrease linearly with pressure to zero at a level $\sigma_u = 0.65$. Thus,

$$F_s = F_{s0} \frac{\sigma - \sigma_u}{1 - \sigma_u} \qquad (5)$$

and

$$F_w = F_{w0} \frac{\sigma - \sigma_u}{1 - \sigma_u} \qquad (6)$$

for $\sigma_u \leq \sigma \leq 1$. The value chosen for σ_u agrees, more or less, with the value of 700 mb employed by Petterssen et al. (1962) for the height of penetration of the fluxes of sensible heat and water vapor. However, Gadd and Keers (1970) assume that only the lowest 100 mb is immediately affected by these transfer processes.

The rate of input of heat per unit mass from sensible heat flux is

$$H_s = \frac{g}{p_s} \frac{\partial F_s}{\partial \sigma} = \frac{g}{p_s} \frac{F_{s0}}{1 - \sigma_u}. \qquad (7)$$

Similarly, the rate of increase of r due to evaporation is

$$W = \frac{g}{p_s} \frac{\partial F_w}{\partial \sigma} = \frac{g}{p_s} \frac{F_{w0}}{1 - \sigma_u}. \qquad (8)$$

Equations (7) and (8) are computed and substituted in eq (1) and (2) at levels 5, 6, and 7. Note that H_s and W are both invariant with height for these three levels.

4. A CASE STUDY

a. General Description

The model is applied to the intense extratropical cyclone of Feb. 24–26, 1965. This same storm was investigated by Danard (1971). One reason for choosing the same depression was to examine the improvements arising from halving the grid size and reducing truncation error.

Numerical predictions are made for 36 hr starting from 1200 GMT on Feb. 24, 1965. Prognoses identified as NL (no lakes) exclude sensible heat transfer and evaporation from water surfaces. In addition, the Great Lakes are treated as land for radiation purposes (Danard 1971). In
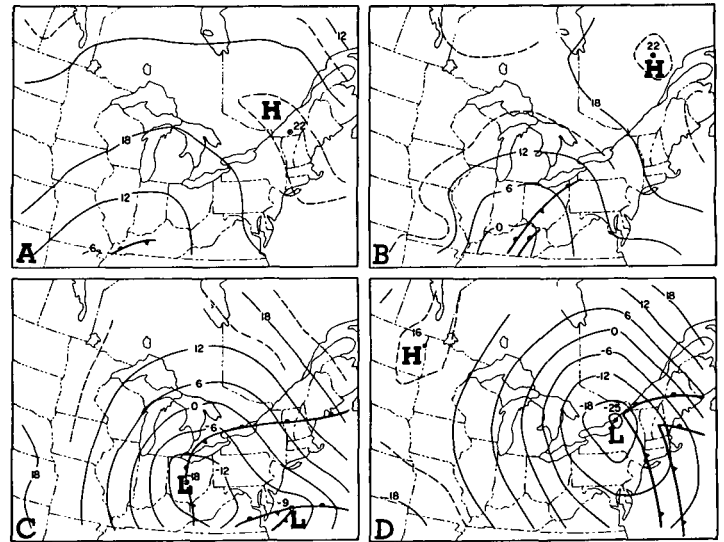

FIGURE 3.—Actual 1000-mb heights in dekameters (dam) for (A) 1200 GMT, Feb. 24; (B) 0000 GMT, Feb. 25; (C) 1200 GMT, Feb. 25; and (D) 0000 GMT, Feb. 26, 1965.

forecasts labeled L (with lakes), these processes are included.

Because the lateral boundaries are only about 1000 km from the borders of the region presented in the forecasts (fig. 2), boundary error is likely to affect the 36-hr predictions, especially in the western areas. Nevertheless, the following results show that the prognoses appear to remain more or less viable for the entire time period.

b. 1000-Mb Heights

The actual 1000-mb charts for the period studied are presented in figure 3. Note the intense cyclone development. Figures 4 and 5 show prognoses made that include effects of water surfaces (L) and exclude these processes (NL). These predictions are much better than those of Danard (1971) for the same storm. The latter employed a grid size twice that of the present study. Otherwise, the computational procedure was identical to that for the NL forecasts.

The effects of the Great Lakes are evident in figure 4 after 36 hr by the extension of the trough to the northwest of the Low. This causes a decrease in pressure gradient immediately to the northwest of the cyclone center and an increase over Lake Superior. The resulting effect on the wind is discussed in subsection 4e. The 1000-mb height differences between the L and NL 36-hr prognoses are shown in figure 6. Heights are lowered by as much as 70 m over the Great Lakes. This is comparable to the maximum surface pressure drop of 6 or 7 mb estimated by Petterssen and Calabrese (1959). Maximum height drops off the east coast are about 50 m.

The orientation of the height difference pattern over the Great Lakes is southeast to northwest. Of interest are the stationary oscillations with the same orientation to the west of the Great Lakes. The amplitude is about 20 m and decreases with increasing distance from the
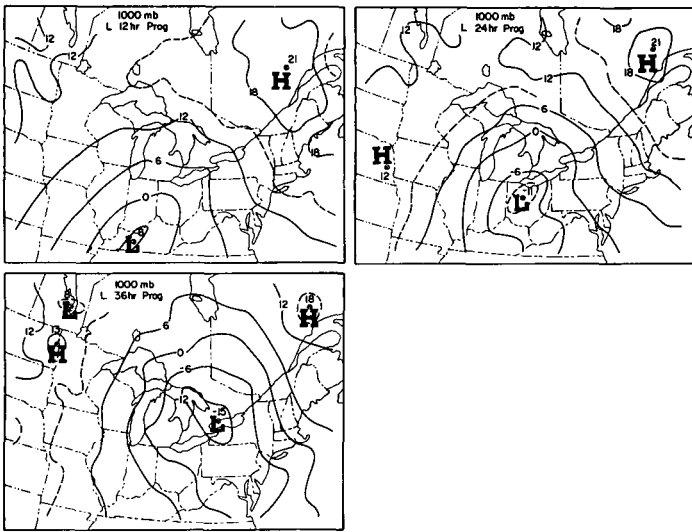
FIGURE 4.—Predicted 1000-mb heights (dam) including effects of water surfaces (L).
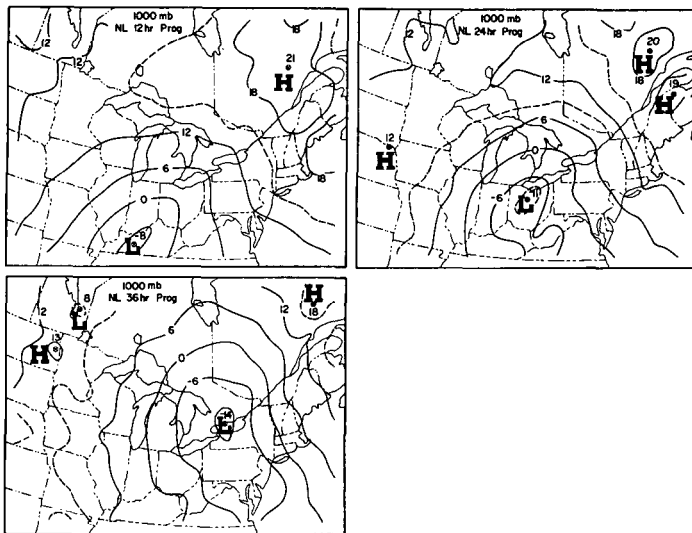

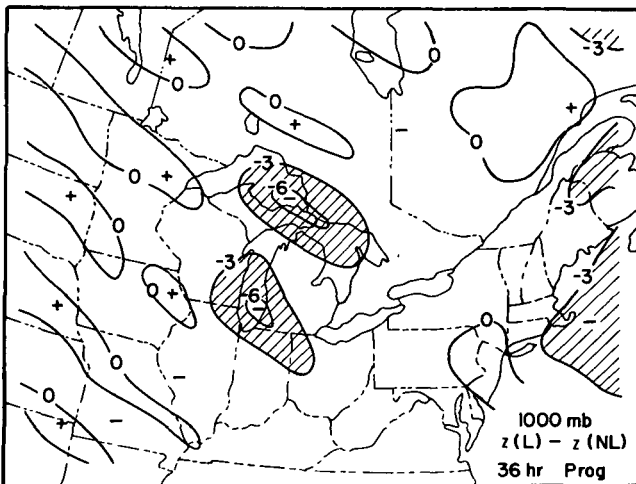FIGURE 5.—Predicted 1000-mb heights (dam) excluding effects of water surfaces (NL).

FIGURE 6.—Difference in 36-hr predicted 1000-mb heights (dam).

TABLE 1.—*Root-mean-square (rms) actual height changes* (R_a) *and rms height errors for prognoses (prog)*

Time	Level	R_a	Prog		
			LG	NL	L
(hr)	(mb)	(m)	(m)	(m)	(m)
12	1000	47	34	34	35
	850	40	26	44	43
	700	40	32	50	48
	500	45	33	72	69
	300	58	91	41	41
24	1000	133	76	49	47
	850	115	70	53	53
	700	101	81	68	68
	500	119	71	101	98
	300	151	80	91	88
36	1000	186	136	64	63
	850	161	138	82	83
	700	167	153	120	122
	500	194	168	173	172
	300	264	172	191	189

lakes. While their origin is undoubtedly mainly numerical, it is possible that similar fluctuations exist in the real atmosphere but with a smaller amplitude. The oscillations are less noticeable to the east of the Great Lakes due to influences of the North Atlantic Ocean. One way to damp these oscillations would be to smooth the transition between Great Lakes data points and surrounding land data points.

c. Statistical Results

Root-mean-square (rms) height changes and rms height errors for the prognoses are shown in table 1. They are calculated from the 12×16 points covering the area in figures 3–11. For comparison, the results of Danard (1971) for the same region are also included. They are identified as LG (large grid) and contain the same physical processes as the NL forecasts.

The most striking feature of table 1 is the reduction in error in the lower troposphere by halving the grid size (compare either the NL or L prognoses with the LG forecasts). Results are, however, slightly worse at 300 mb. This may be attributed to the lack of resolution of the model near the tropopause (fig. 1). Apparently, there are physical processes operating in the upper troposphere in this case whose representation is not improved by reducing horizontal truncation error.

There is no significant difference between the NL and L rms errors. This is to be expected because only a few points are over water.

d. Influences on Temperature and Moisture in the Lower Troposphere

Observed and predicted 850-mb temperatures and dew points are averaged at 36 hr after the forecast was made over the six Great Lakes gridpoints of figure 2. Results are shown in table 2. Both the L and NL prognoses indi-

TABLE 2.—*Average 36-hr observed and predicted 850-mb temperatures and dew points (°C) for the six Great Lakes gridpoints of figure 2*

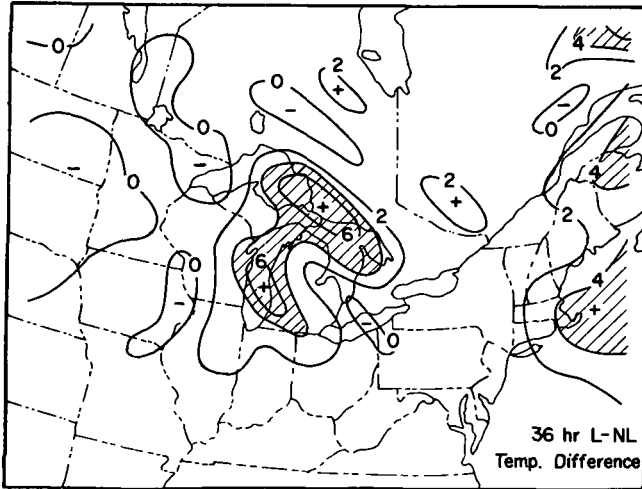|	Observed	Prog	
		L	NL
T	−17	−11	−16
T_d	−23	−11	−16

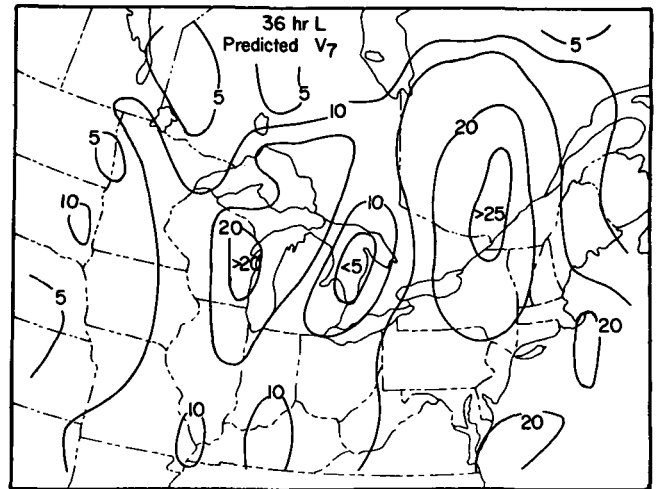FIGURE 7.—Difference in 36-hr predicted mean virtual temperature (°C) from 1000 to 700 mb.

FIGURE 8.—Predicted wind speeds (m/s) at $\sigma=0.98$ after 36 hr including effects of water surfaces.
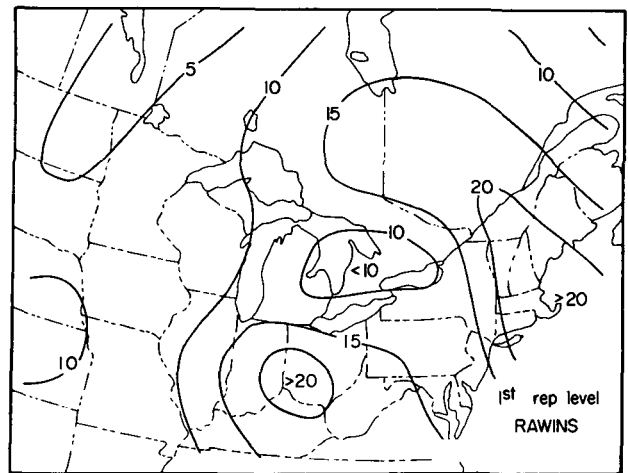

FIGURE 9.—Actual rawinsonde wind speeds (m/s) at the first reportable level at 0000 GMT, Feb. 26, 1965.

cate a higher relative humidity (lower temperature-dew point spread) than observed. The actual surface Low is farther east than predicted by either prognosis (figs. 3–5). This probably explains why actual temperatures are lower than forecast.

Figure 7 shows the difference (L minus NL) in 1000–700-mb mean virtual temperatures between the 36-hr prognoses. These are obtained from the forecast heights at 1000 and 700 mb. Values exceed 7°C over the Great Lakes and 5°C northeast of Cape Cod, Mass. There are also large values in the Gulf of Saint Lawrence and off the Labrador coast. There are a few areas of negative temperature difference, but their magnitude is small (less than 1°C).

e. Wind Speeds in the Ekman Layer

Figure 8 shows the 36-hr L forecast wind speeds at $\sigma=0.98$. This level is about 200 m above the earth's surface. Note the strong winds over the Saint Lawrence River Valley and Wisconsin.

Figure 9 shows actual wind speeds for the verifying time at the first reportable level (1,000 or 2,000 ft above sea level, except for the western region). This level corresponds approximately to $\sigma=0.98$ although it is not a fixed distance above the earth's surface. Pilot balloons are normally not released during inclement weather; therefore, only rawinsonde data are available in the vicinity of the cyclone. Because this is the region of chief interest, it did not seem worthwhile to include pilot balloon winds

in other areas. Thus, figure 9 was constructed solely from rawinsonde data. In addition, several key stations were missing (notably Maniwaki, Nitchequon, and Seven Islands, Quebec, and Portland, Maine). These limitations should be borne in mind when using figures 8 and 9. The most notable fault of figure 8 is the absence of strong winds south of the Great Lakes, partially caused by the underestimate of horizontal pressure gradient there (cf. figs. 3 and 4). Probably an additional factor is the destabilization and mixing in the real atmosphere from surface heating as the air flows southward over land. This results in a high ratio of low-level to geostrophic wind speeds. This effect is not included in the numerical model.

The difference in predicted wind speeds at $\sigma=0.98$ after 36 hr caused by including effects of water surfaces may be seen in figure 10. Speeds are reduced by up to 6 m/s over Michigan and Lake Huron. Increases of the same magnitude are found over Wisconsin and Lake Superior. This pattern is to be expected from the influences of the Great Lakes on 1000-mb heights (subsection 4b). Speeds are also decreased by more than 6 m/s east of Delaware and augmented by up to 5 m/s in the Gulf of Saint Lawrence.

f. Precipitation

Figure 11 shows the 0–36-hr observed precipitation and the L forecast amounts. The predicted difference (L−NL) when effects of water surfaces are included is given in figure 12. Observed values are obtained by computing averages over squares with sides equal to one grid length (190 km at 60°N) centered on each gridpoint. Comparing these results with those of Danard (1971), one sees that the prediction is considerably improved by halving the grid size.

The influence of water surfaces on predicted precipitation after 36 hr (fig. 12) amounts to about 0.5 cm over Lake Huron, 0.4 cm over Lake Michigan, and 0.6 cm east of Delaware. This represents only the effect on precipitation associated with large-scale vertical motion. Small-scale convection is not included in the model. However, a check of the 36-hr L predicted temperatures at 850 and 500 mb shows that the lapse rate is less than moist adiabatic over the Great Lakes gridpoints. Nevertheless, the problem of convective precipitation is important enough to warrant further study. Continuity requires downward motion in the vicinity of regions of ascent. This is manifest by the reduction in precipitation over Ohio, Pennsylvania, and New York.

The area of enhanced precipitation off the United States coast is south of the maximum temperature rise and 1000-mb height fall (figs. 6 and 7). However, the corresponding areas over the Great Lakes are in approximately the same locations in figures 6, 7, and 12. Apparently, the effect on precipitation is appreciable only where preexisting upward motion exists and not necessarily where sensible heat flux is largest.

The average 36-hr predicted and observed precipitation amounts over the six Great Lakes gridpoints of figure 2 are given in table 3. Observed amounts are estimated from values at land stations. While both the L and NL prognoses underforecast the precipitation, the former is closer to reality. The underprediction is consistent with the underestimate of the storm's intensity (subsection 4b).

TABLE 3.—*Average observed and predicted 36-hr precipitation amounts (cm) for the six Great Lakes gridpoints of figure 2*

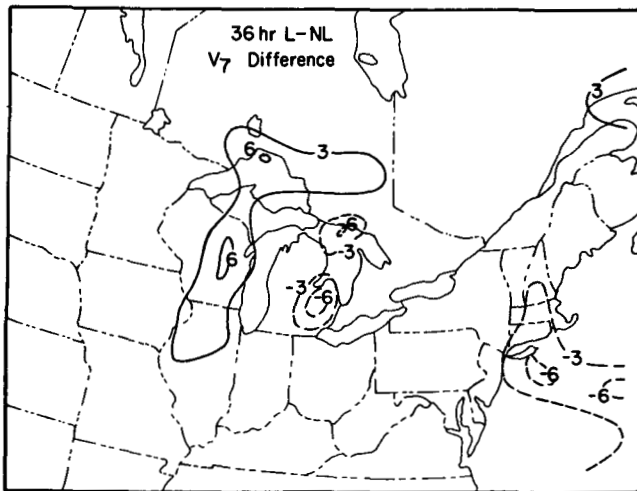| Observed	Prog	
	L	NL
1. 2	0. 7	0. 4

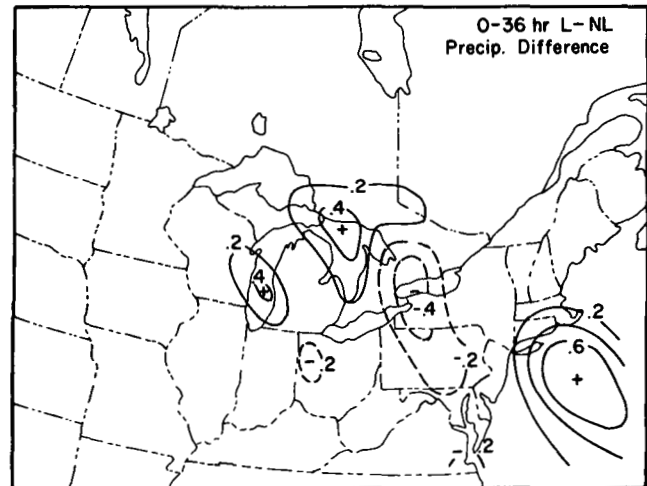FIGURE 10.—Difference in 36-hr predicted wind speeds (m/s) at $\sigma = 0.98$.

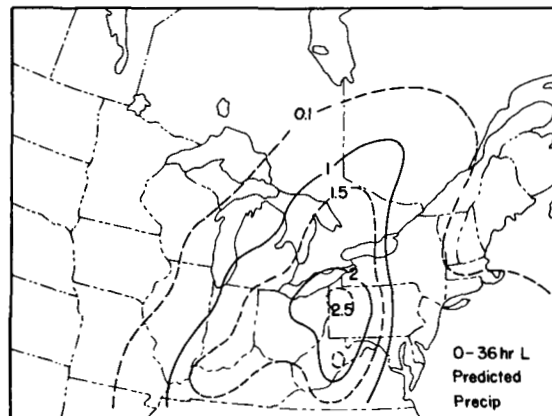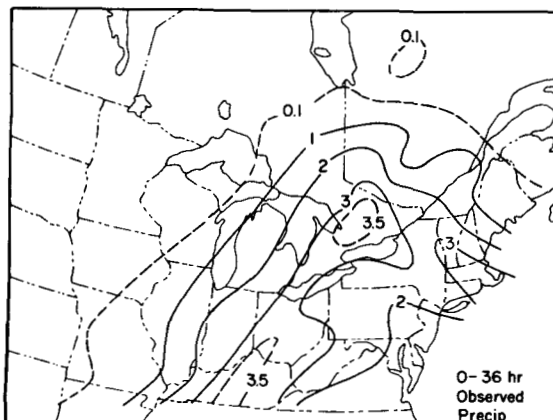FIGURE 12.—Difference in 36-hr predicted precipitation (cm).

FIGURE 11.—Observed 36-hr precipitation (cm) and predicted 36-hr amounts including effects of water surfaces.

TABLE 4.—*Average 36-hr observed and predicted isobaric heights (m) for the six Great Lakes gridpoints of figure 2*

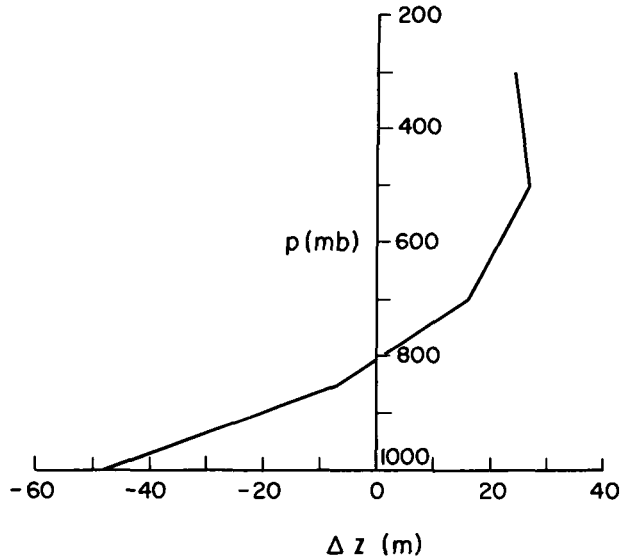| Level (mb)	Observed	Prog	
		L	NL
1000	−10	−62	−14
850	1223	1186	1193
700	2681	2678	2661
500	5165	5162	5135
300	8658	8671	8647

FIGURE 13.—Average 36-hr predicted isobaric height differences (m) over the Great Lakes (with water surfaces minus without water surfaces).
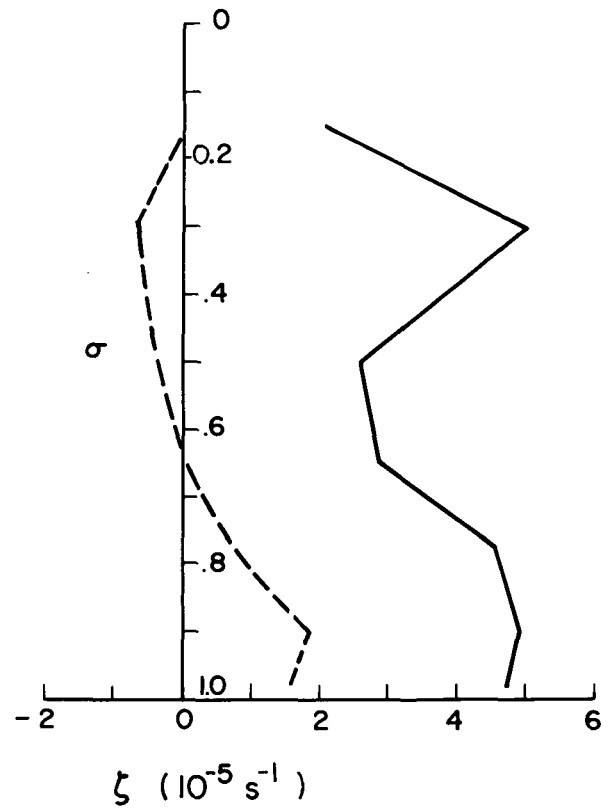

FIGURE 14.—Average 36-hr predicted vorticity (solid line) over the Great Lakes including effects of water surfaces and predicted vorticity differences (dashed line) with water surfaces minus without water surfaces.

g. Vertical Variation of Effects on Heights of Isobaric Surfaces, Vorticity, and Divergence

The 36-hr observed and predicted isobaric heights are averaged over the six points representing the Great Lakes. Values are computed at 1000, 850, 700, 500, and 300 mb and are presented in table 4. The L forecast heights are closer to the actual at 700 and 500 mb while the NL predictions are better at 1000, 850, and 300 mb.

The 36-hr average height differences (L minus NL) for the Great Lakes gridpoints are shown in figure 13. Below about 800 mb, the Great Lakes cause a lowering of the isobaric heights (48 m at 1000 mb). However, at higher levels, isobaric heights are raised (27 m at 500 mb).

The 36-hr L forecast vorticities and divergences on sigma surfaces of the wind are also averaged over the Great Lakes gridpoints. Values at the seven sigma levels above the surface as well as differences in vorticity and divergence (L minus NL) are presented in figures 14 and 15.

The predicted relative vorticity is $4.9 \times 10^{-5} \text{s}^{-1}$ at $\sigma = 0.9$ (fig. 14). There is another maximum of $5 \times 10^{-5} \text{s}^{-1}$ at $\sigma = 0.3$. The influence of the Great Lakes (dashed curve) amounts to $1.9 \times 10^{-5} \text{s}^{-1}$ at $\sigma = 0.9$ and decreases
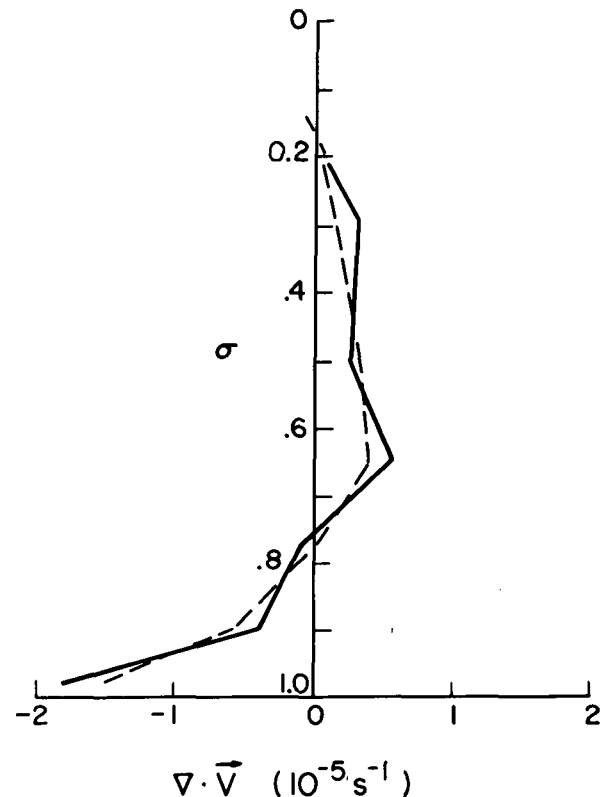

FIGURE 15.—Average 36-hr predicted divergence (solid line) over the Great Lakes including effects of water surfaces and predicted divergence differences (dashed line) with water surfaces minus without water surfaces.
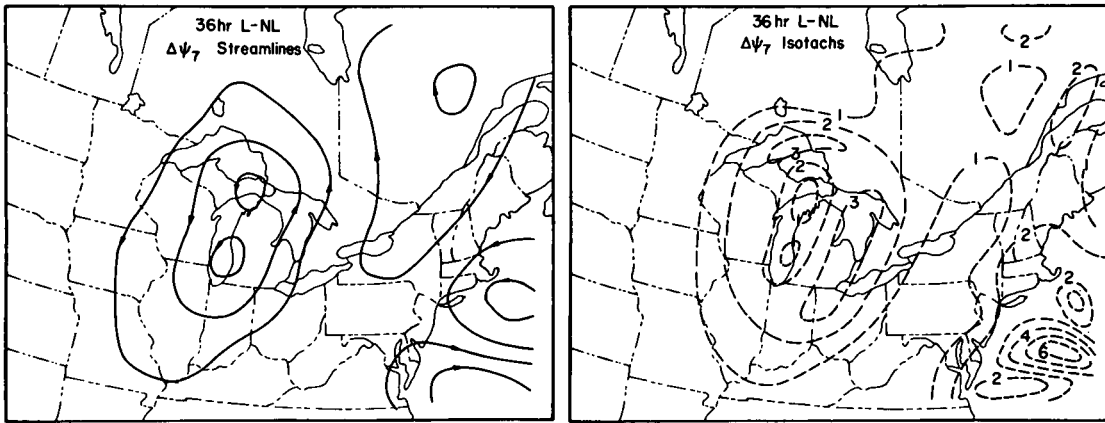
FIGURE 16.—Streamlines and isotachs (m/s) of rotational part of 36-hr predicted wind difference at $\sigma = 0.98$.
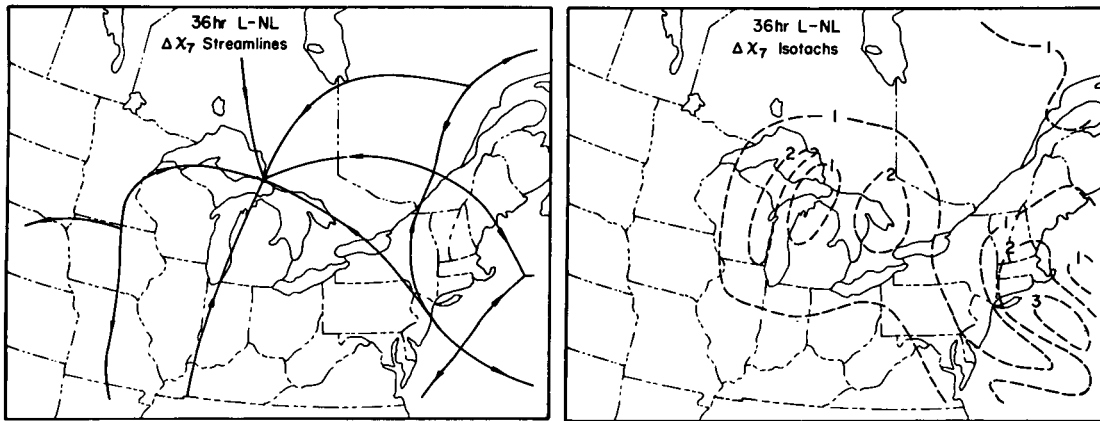

FIGURE 17.—Streamlines and isotachs (m/s) of divergent part of 36-hr predicted wind difference at $\sigma = 0.98$.

to zero at about $\sigma = 0.65$. At higher levels, relative vorticity is negative, attaining a value of $-0.6 \times 10^{-5} \mathrm{s}^{-1}$ at $\sigma = 0.3$. These figures may be compared to the effect at 1000 mb estimated by Petterssen and Calabrese (1959) of $4 \times 10^{-5} \mathrm{s}^{-1}$ after 48 hr. Thus, the Great Lakes contribute significantly to relative vorticity in the lower troposphere.

The predicted divergence (fig. 15) is $-1.8 \times 10^{-5} \mathrm{s}^{-1}$ (i.e., convergence) at $\sigma = 0.98$. The level of nondivergence is at about $\sigma = 0.75$. Above this level, the divergence is positive, reaching a value of $0.6 \times 10^{-5} \mathrm{s}^{-1}$ at $\sigma = 0.65$. The effect of the Great Lakes (dashed curve) has a similar vertical variation and essentially the same magnitude as the total divergence (i.e., Great Lakes plus other causes). The extrema are $-1.5 \times 10^{-5} \mathrm{s}^{-1}$ at $\sigma = 0.9$ and 0.4×10^{-5} at $\sigma = 0.65$.

Summarizing, it is seen that the Great Lakes significantly lower the isobaric heights and increase the relative vorticity and convergence in the lower troposphere. However, these influences are reversed in sign in the upper troposphere.

h. Effects on Rotational and Divergent Winds in the Ekman Layer

As is seen from figures 14 and 15, the effects of the Great Lakes on both vorticity and divergence are large at $\sigma = 0.98$. This fact will be explored further.

According to a theorem by Helmholtz, a general two-dimensional vector **A** can be written as the sum of a rotational (nondivergent) vector and a divergent (irrotational) one. Thus, taking **A** to be horizontal,

$$\mathbf{A} = \mathbf{k} \times \nabla \psi - \nabla \chi \tag{9}$$

where ψ is the stream function and χ is the velocity potential. These are found by relaxation from the equations

$$\nabla^2 \psi = \mathbf{k} \cdot \nabla \times \mathbf{A} \tag{10}$$

and

$$\nabla^2 \chi = -\nabla \cdot \mathbf{A}. \tag{11}$$

Here, **A** is the vector wind difference at $\sigma = 0.98$ between 36-hr prognoses with and without effects of water surfaces (i.e., L minus NL).

Results are shown in figures 16 and 17. From figures 7 and 16 we see that cyclonic vortexes are created in regions where heat input is large (Great Lakes and east of Cape Cod, Mass.). These regions are also areas of convergence (fig. 17). Compensating anticyclonic vortexes are found over central Quebec and east of Cape Hatteras, N.C. Areas of divergence are located north of the Gulf of Saint Lawrence and east of Maryland. The magnitude of the divergent vector is generally a bit less than that of the rotational part. Both have maxima of about 3 m/s near the Great Lakes.

5. CONCLUDING REMARKS

The main purpose of this paper has been to elucidate the large-scale effects of the Great Lakes on a major winter cyclone. The grid size (190 km) precludes delineation of small-scale phenomena such as snowbelts. After 36 hr, maximum influences are as follows: temperatures in the lower troposphere are increased 7°C, 1000-mb heights are decreased 70 m, Ekman layer wind speeds are modified by 6 m/s, precipitation is increased 0.5 cm, and rotational and divergent winds both are changed by 3 m/s near the earth's surface. In addition, effects on heights of isobaric surfaces, vorticity, and divergence have opposite signs in the lower and upper troposphere. With the exception of precipitation, the above values may appear large. However, it must be remembered that surface winds are very strong during the period, and fluxes of both heat and water vapor are directly proportional to wind speed [eq (3) and (4)].

The treatment of vertical mixing (i.e., convection) probably most needs improvement in this model. To be sure, the instantaneous penetration of the fluxes of sensible heat and water vapor from water surfaces to $\sigma=0.65$ (sec. 3) does imply strong mixing at low levels. Nevertheless, it is desirable to account for these processes in a physically more realistic way. In particular, the addition of convective precipitation and the accompanying stabilizing effect would be advantageous. Methods to do so include convective adjustment as described by Manabe et al. (1965) and the technique of Krishnamurti and Moxim (1971) based on moisture convergence in the Ekman layer. Gadd and Keers (1970) employ a modification of the former procedure.

Another area where improvement is desirable is vertical resolution and initial data near the tropopause. As is shown in subsection 4c, halving the grid size greatly improves the predictions at low levels but not in the upper troposphere.

REFERENCES

Berkofsky, Louis, and Bertoni, Eugene A., "Topographic Charts at One-Degree Intersections for the Entire Earth," *U.S. Air Force Geophysics Research Directorate Notes* No. 42, Air Force Cambridge Research Laboratories, Bedford, Mass., Sept. **1960**, 43 pp.

Cressman, George P., "Improved Terrain Effects in Baroclinic Forecasts," *Monthly Weather Review*, Vol. 88, Nos. 9–12, Sept.–Dec. **1960**, pp. 327–342.

Danard, Maurice B., "A Numerical Study of the Effects of Long-wave Radiation and Surface Friction on Cyclone Development," *Monthly Weather Review*, Vol. 99, No. 11, Nov. **1971**, pp. 831–839.

Gadd, A. J., and Keers, A. F., "Surface Exchanges of Sensible and Latent Heat in a 10-level Model Atmosphere," *Quarterly Journal of the Royal Meteorological Society*, Vol. 96, No. 408, London, England, Apr. **1970**, pp. 297–308.

Krishnamurti, Tiruvalem N., and Moxim, Walter J., "On Parameterization of Convective and Nonconvective Latent Heat Release," *Journal of Applied Meteorology*, Vol. 10, No. 1, Feb. **1971**, pp. 3–13.

Manabe, Syukuro, Smagorinsky, Joseph, and Strickler, Robert F., "Simulated Climatology of a General Circulation Model With a Hydrologic Cycle," *Monthly Weather Review*, Vol. 93, No. 12, Dec. **1965**, pp. 769–798.

Petterssen, Sverre, "Some Aspects of the General Circulation of the Atmosphere," *Centenary Proceedings of the Royal Meteorological Society*, London, England, **1950**, pp. 120–155.

Petterssen, Sverre, *Weather Analysis and Forecasting, Vol. 1: Motion and Motion Systems*, 2d Ed., McGraw-Hill Book Co., Inc., New York, N.Y. **1956**, 428 pp.

Petterssen, Sverre, Bradbury, Dorothy L., and Pedersen, Kaare, "The Norwegian Cyclone Models in Relation to Heat and Cold Sources," *Geofysiske Publikasjoner*, Vol. 24, Oslo, Norway, **1962**, pp. 243–280.

Petterssen, Sverre, and Calabrese, P. A., "On Some Weather Influences Due to Warming of the Air by the Great Lakes in Winter," *Journal of Meteorology*, Vol. 16, No. 6, Dec. **1959**, pp. 646–652.

Rao, Gandikota V., and Danard, Maurice B., "A Review of Some Recent Observational and Dynamical Studies of Lake-Effect Winter Disturbances," *Atmosphere*, Vol. 9, No. 1, University of Toronto Press, Ontario, Canada, **1971**, pp. 26–31.

Richards, T. L., and Irbe, J. G., "Estimates of Monthly Evaporation Losses From the Great Lakes 1950 to 1968 Based on the Mass Transfer Technique," *Proceedings of the Twelfth Conference on Great Lakes Research, Ann Arbor, Michigan, May 5–7, 1969*, International Association of Great Lakes Research, Ann Arbor, Mich., **1969**, pp. 469–487.

Roll, Hans Ulrich, *Physics of the Marine Atmosphere*, Academic Press, New York, N.Y., **1965**, 426 pp.